ELSEVIER

Journal of Nuclear Materials 281 (2000) 117–128

journal of nuclear materials

www.elsevier.nl/locate/jnucmat

A method for determining an effective porosity correction factor for thermal conductivity in fast reactor uranium–plutonium oxide fuel pellets

Masaki Inoue *, Kazuyuki Abe, Isamu Sato

Oarai Engineering Center, Japan Nuclear Cycle Development Institute, 4002 Narita-cho, Oarai-machi, Higashi-ibaraki-gun, Ibaraki-ken, 311-1393, Japan

Received 10 February 2000; accepted 5 July 2000

Abstract

A reliable method has been developed for determining an effective porosity correction factor for calculating a realistic thermal conductivity for fast reactor uranium–plutonium (mixed) oxide fuel pellets. By using image analysis of the ceramographs of transverse sections of mixed-oxide fuel pellets, the fuel morphology could be classified into two basic types. One is a 'two-phase' type that consists of small pores dispersed in the fuel matrix. The other is a 'three-phase' type that has large pores in addition to the small pores dispersed in the fuel matrix. The pore sizes are divided into two categories, large and small, at the 30 μm area equivalent diameter. These classifications lead to an equation for calculating an effective porosity correction factor by accounting for the small and large pore volume fractions and coefficients. This new analytical method for determining the effective porosity correction factor for calculating the realistic thermal conductivity of mixed-oxide fuel was also experimentally confirmed for high-, medium- and low-density fuel pellets.

PACS: 44.30.+v; 28.41.B

1. Introduction

A reliable method for determining an effective porosity correction factor on thermal conductivity has been developed for mixed-oxide fuel for fast reactors. This analytical method was based on prior studies, image and finite element method analyses of fuel matrix-porosity systems, and verified with out-of-reactor experimental measurements.

It is, of course, known that porosity in oxide fuel pellet lowers the thermal conductivity and that the degree of degradation depends on the porosity volume fraction and morphology [1]. Porosity morphology can change significantly in fabrication processes, especially with pore former additions that affect the size, shape and distribution. Some examples illustrating the morphological variances in Japan Nuclear Cycle Development Institute (JNC) fabricated fuels are shown in the ceramographs in Fig. 1 for a high-density fuel pellet (~95%TD), Fig. 2 for a medium-density (~92%TD), and Fig. 3 for a low-density (~85%TD).

The porosity effect on thermal conductivity is one of the most difficult properties to characterize. As a result, direct measurements had to be made on the fabricated fuels to obtain credible values. For reliable thermal analysis of fast reactor fuel pins, particularly at beginning of irradiation conditions, it is imperative that physical property input is accurate. The uncertainty in this parameter relates to the variances in the pore morphology of fuel pellets. Effective porosity correction factors on thermal conductivity must be determined by a reliable method to have realistic thermal analyses using

* Corresponding author. Tel.: +81-29 267 4141; fax: +81-29 267 7130.

E-mail address: minoue@oec.jnc.go.jp (M. Inoue).

0022-3115/00/$ - see front matter
PII: S0022-3115(00)00243-9

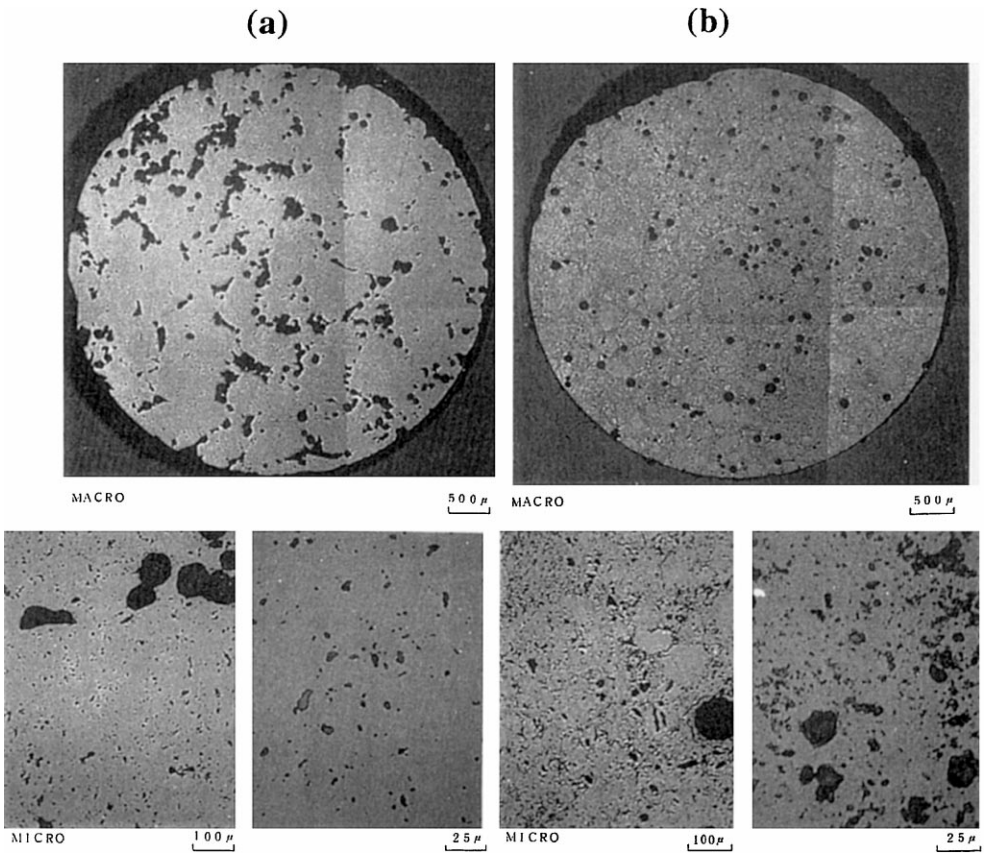

Fig. 1. Macro and micro structure of low density fuel pellets fabricated by JNC: ((a) Lot No. L4; (b) lot No. L5).

established equations, such as those formulated for fully dense fuel [2–4].

The fuel pellet porosity was evaluated by image analysis of optical ceramographs to characterize the morphology and develop a method for determining an accurate and reliable porosity correction factor. Verification of the reliability of this method was obtained by comparing it with actual thermal conductivity measurements of three different lots of fuel pellets.

2. Review of the past studies

2.1. Theoretical studies

The basic equation that has been commonly used to calculate the thermal conductivity of porous oxide fuel pellets is as follows:

$$k = k_0 F, \tag{1}$$

where k is effective thermal conductivity, k_0 is thermal conductivity of fully dense condition, F is effective porosity correction factor. Historically, there have been three major formulas used to calculate the effective porosity correction factor F. These are the 'modified Loeb' (Eq. (2)) with the coefficient α [5], 'Maxwell–Eucken' (Eq. (3)) with the coefficient β, and the Schultz (Eq. (4)) with the coefficient γ [6] as follows:

$$F = 1 - \alpha P, \tag{2}$$

$$F = \frac{1 - P}{1 + \beta P}, \tag{3}$$

$$F = (1 - P)^{\gamma}, \tag{4}$$

where P is the volume fraction of porosity.

2.2. Experimental studies

Nikolopoulos and Ondracek [7] studied the effects of porosity on thermal conductivity and proposed the 'Bound Concept'. This concept characterized porous fuel pellets as if they were isotropic that the coefficient γ was 1.5–3.0. Schultz [6] theorized that, for spherical pores distributed randomly, γ should be 1.5. However, in actuality the coefficients for fuel pellets are larger ($\gamma > 1.5$),

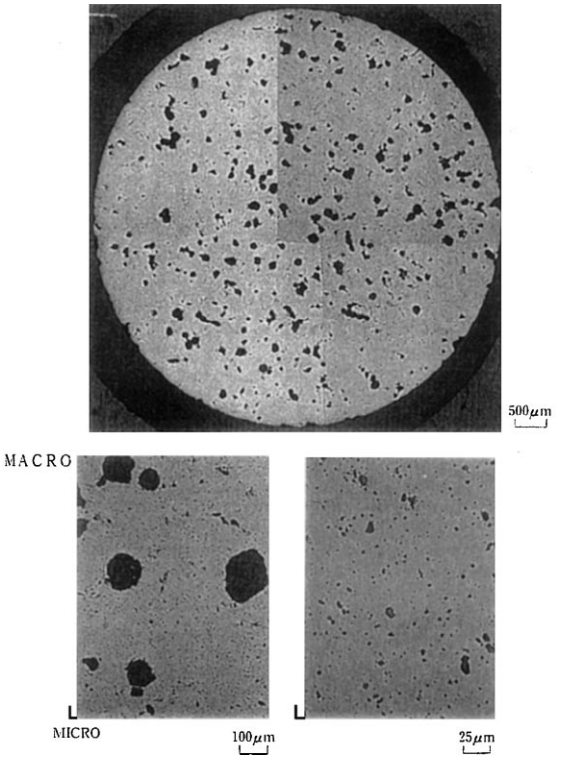

Fig. 2. Macro and micro structure of medium density fuel pellet fabricated by JNC (Lot No. M4).

due to the porosity being neither spherical nor uniformly distributed [1]. The IAEA [8] recommended $\alpha = 2.5 \pm 1.5$ for the modified Loeb equation for $0 < P < 0.1$. Shimizu and Hirai [9] experimentally showed that $\gamma = 2.4$ for $0.044 < P < 0.470$. Kobayashi [10] attempted to interpret the phenomena by considering the local distortions in fine pores along grain boundaries and found that $\beta = 2$.

The IAEA recommendation ($\alpha = 2.5 \pm 1.5$) is in agreement with other experimenters [9,10]. Experimentally the porosity effect on thermal conductivity in high-density uranium dioxide fuel pellets ($P < 0.1$) has been well characterized, even though the mechanism is not clear.

2.3. Analytical model

An analytical model for determining the effective porosity correction factor for a universal fuel pellet was proposed by Harding et al. (Eq. (5)):

$$F = (1 - P_1)(1 - P_2 - P_3)^{2.5}(1 - P_4 - P_5)^{3.5}, \quad (5)$$

where volume fraction P_1 is for spherical pores greater than 5 μm in diameter, P_2 is for fine spherical manufacturing pores, P_3 is for fine spherical intragranular gas bubbles or pores, and P_4 is lenticular grain face bubbles or pores and P_5 is for toroidal grain edge bubbles or pores; the terms 'fine' refers to less than 5 μm in diameter [11]. However, Harding's model requires detailed characterizations of the fuel pellets and is, therefore, considered impracticable for determining the effective porosity correction factor.

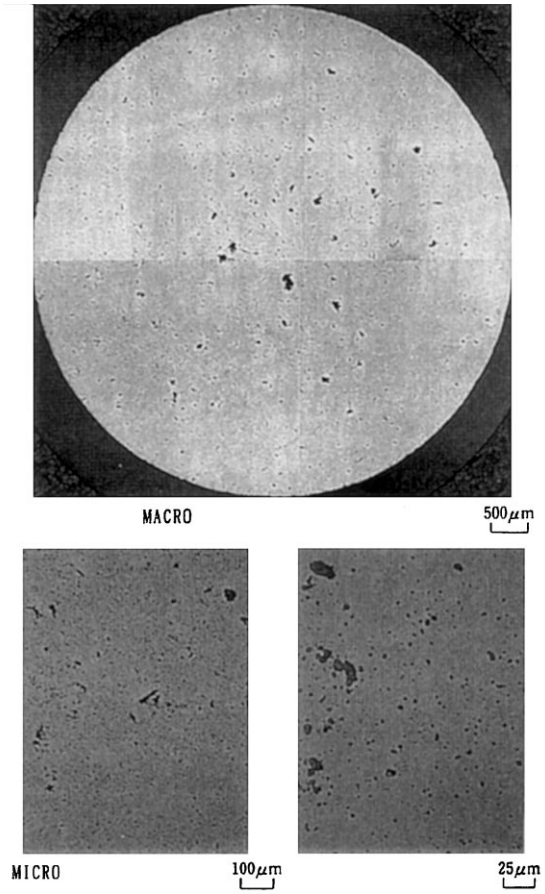

Fig. 3. Macro and micro structure of high density fuel pellet fabricated by JNC (Lot No. H1).

3. Investigations of effective porosity correction factor

3.1. Fuel pellets from short-term irradiation tests

Six short-term irradiation tests were conducted in the experimental fast reactors JOYO and EBR-II, and were identified as 'B4M', 'B5D-1', 'B5D-2', 'INTA-1', 'INTA-2', and 'P-E01' [12–15]. The fuel pellets were fabricated to the specifications summarized in Table 1. The B4M, INTA-1, and P-E01 tests used 'MONJU' type fuel pins containing fuel pellets with about 30 mass% Pu, an oxygen-to-metal ratio of 1.97, and a nominal density of 85%TD. The tests B5D-1, B5D-2, and INTA-2 used

Table 1
Specifications of the fuel pellets for short term irradiation tests

	Irradiation test	Lot No.	Density level	Pore former addition	Density (lot mean) %TD	Pu content Pu/(Pu + U) (lot mean) mass%	Oxygen-to-metal ratio (lot mean)
1	Joyo driver	J1	High	No	92.73	28.62	1.97
2	Joyo driver	J2	High	No	93.52	28.97	1.98
3	Joyo driver	J3	High	No	92.41	27.80	1.98
4	Joyo driver	J4	High	No	93.33	28.40	1.97
5	Joyo driver	J5	High	No	93.14	28.53	1.97
6	Joyo driver	J6	High	No	92.68	28.64	1.97
7	Joyo driver	J7	High	No	93.21	28.70	1.98
8	Joyo driver	J8	High	No	91.93	28.79	1.99
9	Joyo driver	J9	High	No	93.34	28.40	1.97
10	Joyo driver	J10	High	No	93.15	28.13	1.96
11	Joyo driver	J11	High	No	93.13	28.01	1.97
12	Joyo driver	J12	High	No	93.57	28.47	1.97
13	Joyo driver	J13	High	No	92.64	28.29	1.97
14	Joyo driver	J14	High	No	92.97	28.29	1.97
15	Joyo driver	J15	High	No	93.32	28.27	1.97
16	Joyo driver	J16	High	No	93.19	28.45	1.97
17	Joyo driver	J17	High	No	93.06	28.15	1.97
18	Joyo driver	J18	High	No	93.02	28.87	1.99
19	B5D-2	H1	High	No	95.20	19.37	1.97
20	INTA-2	H2	High	No	95.38	18.89	1.96
21	INTA-2	H3	High	No	94.46	19.16	1.99
22	B5D-1	M1	Medium	Yes	91.03	19.0	1.96
23	B5D-2	M2	Medium	Yes	91.36	19.50	1.98
24	B5D-2	M3	Medium	Yes	91.56	19.46	1.96
25	INTA-2	M4	Medium	Yes	91.95	19.16	1.99
26	INTA-2	M5	Medium	Yes	92.35	18.89	1.95
27	INTA-2	M6	Medium	Yes	91.70	18.89	1.96
28	INTA-2	M7	Medium	Yes	92.07	18.89	1.95
29	B4M	L1	Low	Yes	85.92	29.68	1.95
30	B4M	L2	Low	Yes	84.64	29.45	1.96
31	INTA-1	L3	Low	Yes	85.18	29.55	1.96
32	INTA-1	L4	Low	Yes	84.19	29.97	1.97
33	INTA-1	L5	Low	Yes	85.48	29.93	1.97
34	INTA-1	L6	Low	Yes	86.04	29.69	1.95
35	P-E01	L7	Low	Yes	86.51	29.37	1.99

'Large Diameter' type fuel pins with 19 mass% Pu, an oxygen-to-metal ratio of 1.94 and 1.97, and nominal densities of 92% or 95%TD.

The fuel pellet fabrication lot identifications were as follows: lots H1–H3 of high-density pellets (~95%TD), lots M1–M7 of medium-density pellets (~92%TD), lots L1–L7 of low-density (~85%TD) pellets, and lots J1–J18 of JOYO driver pellets (~93%TD). For porosity comparison purposes the JNC fabricated 'JOYO Mk-II driver first-load fuel pellets' were selected as the reference: 28.5 mass% Pu, 1.97 oxygen-to-metal ratio, and a 93%TD nominal density.

Figs. 1–3 show some typical ceramographs of MONJU type and Large Diameter type fuel pellets. Differences of the porosity morphology in the same fabrication density specification can be seen in Figs. 1(a) and (b).

3.2. Porosity distribution

The distribution of given sizes of porosity was determined by performing an image analysis of ceramographs of the fuel pellet transverse section and then the pore sizes were divided into four categories of area equivalent diameters, where 'Fine' is smaller than 5 μm; 'Medium' ranges from 5 to 10 μm; 'Coarse' ranges from 10 to 30 μm; 'Large' is larger than 30 μm. For convenience, the 'Fine', 'Medium' and 'Coarse' pores are collectively called as 'small pores' in this study. The criteria for 'Fine' pores were selected in accordance with

Harding's classification and the average grain size (6 μm) of the JOYO driver fuel pellets. The 'Medium' and 'Coarse' were arbitrarily selected as size factors of 2 and 6, respectively. As seen in Figs. 1 and 2, the diameters of the large pores, which were formed by a pore former, are usually greater than 30 μm.

The number density (pores per unit area) and area fraction of the pores in the high magnification ceramographs (one or two per lot) were image analyzed based on the above classifications and the results are summarized in Table 2 (the number densities are normalized into per 10^4 μm^2 units in the table). It should be noted that the area fraction of porosity at an arbitrary section was assumed equal to the volume fraction.

In high-density fuel pellets (lots H1–H3) the area fractions were nearly equal to those by geometric density. This indicates that these lots were two phased, fuel matrix plus small pores, and defined as a 'two-phase' type morphology (Fig. 4(a)).

In medium-density fuel pellets (lots M1–M7) both the number densities and the area fractions of small pores were comparable to those in the two-phase high-density fuel. However, large pores were also dispersed in this basic two-phase type fuel. This dual pore size type of porosity in the fuel matrix was referred to as a 'three-phase' type morphology, as illustrated in Fig. 4(b).

The low-density fuel pellets (lots L1–L4) were also categorized as three-phase type because of the similarity in the distribution of small pores with the high-density fuel pellets. Furthermore, lots L5 and L6 were also categorized as a three-phase system, because the distribution of small pores was comparable to the JOYO driver fuel. In lot L7 the area fraction of small pores was nearly equal to that by geometric density and therefore was categorized as 'two-phase' type.

3.3. Analytical model for JNC fabricated fuel pellets

The morphologies of the fuel pellets in the short-term irradiation tests was categorized into 'two-phase' and 'three-phase' types, as discussed in Section 3.2. Considering these two types and the synergy of the modified Loeb formula, the following equation (Eq. (6)) was proposed to determine an effective porosity correction factor:

$$F = (1 - \alpha_L P_L)(1 - \alpha_s P_s), \tag{6}$$

where F is the effective porosity correction factor, α_S is a coefficient for small pores, α_L is a coefficient for large pores, P_S is the volume fraction of small pores and P_L is volume fraction of large pores. In 'two-phase' type fuel pellets like those in lots H1–H3 and L7, P_L is 0. But, before applying Eq. (6) to the thermal conductivity equation, two other coefficients (α_S and α_L) must be determined. The effect of small pores on thermal conductivity has been well characterized in past studies as described in Section 2.2. Martin suggested that the coefficient, which has been recommended for uranium dioxide, might also be applied to mixed oxide fuel [1]. It is on this basis that $\alpha_S = 2.5$ should be used in Eq. (6). Since the large pores are not spherical nor uniformly distributed, the coefficient α_L must be determined by an alternative method. In the absence of reference studies, the coefficient α_L for large pores had to be determined by theoretical methods and experimentally verified.

3.4. FEM analysis to determine the coefficient: α_L

A theoretical approach for determining the coefficient α_L by a numerical analysis with finite element methods (FEM) was accomplished by using the FINAS code [16] to calculate the heat flow in porous bodies. This two-dimensional steady-state thermal analysis was performed on the large pores dispersed in the matrix.

Five ceramographs showing typical large pores were selected from medium- and low-density fuel pellets and nine mm^2 squares with FEM mesh was

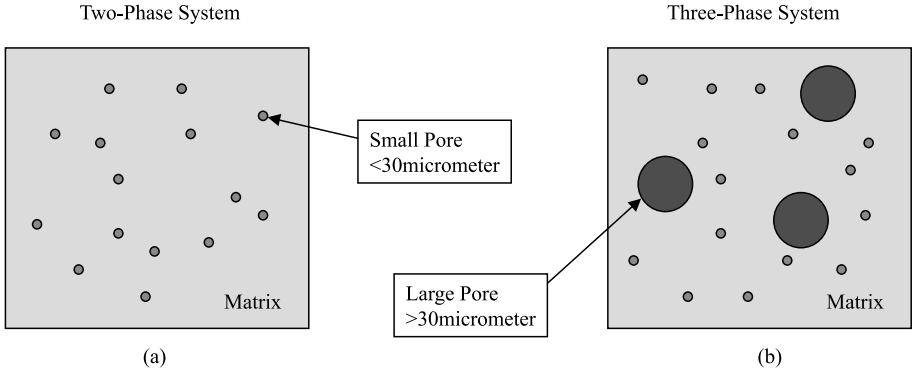

Fig. 4. Schematics of two-phase and three-phase system.

Table 2
Results of image analysis and effect on thermal conductivity

	Test name	Lot No.	Number density[a] of 'Fine' pores ≦5 μm[b]	Number density[a] of 'Medium' pores 5–10 μm[b]	Number density[a] of 'Coarse' pores 10–30 μm[b]	Total porosity volume, $P = PL + PS$ (%)	Porosity volume by large pores >30 μm[b], $PL = P - PS$ (%)	Porosity volume by small pores ≦30 μm[b], PS (%)	Grain size (μm)	Classification	Effective porosity correction factor (predicted), F
1	Joyo driver	J1	152.9	9.5	0.0	7.27	0.33	6.94	4	Two-phase	–
2	Joyo driver	J2	67.5	7.9	1.2	6.48	−1.91	8.39	9	Two-phase	–
3	Joyo driver	J3	106.4	5.9	2.0	7.59	0.07	7.52	10	Two-phase	–
4	Joyo driver	J4	69.3	3.2	2.1	6.67	0.20	6.47	6	Two-phase	–
5	Joyo driver	J5	46.7	3.9	1.5	6.86	1.29	5.57	9	Two-phase	–
6	Joyo driver	J6	153.0	3.7	0.0	7.32	3.35	3.97	2	Two-phase	–
7	Joyo driver	J7	161.1	3.5	0.0	6.79	2.54	4.25	4	Two-phase	–
8	Joyo driver	J8	88.8	5.4	1.0	8.07	1.71	6.36	15	Two-phase	–
9	Joyo driver	J9	107.0	1.0	2.0	6.66	−1.00	7.65	4	Two-phase	–
10	Joyo driver	J10	161.3	1.8	1.2	6.85	2.32	4.53	1	Two-phase	–
11	Joyo driver	J11	85.8	5.5	0.4	6.87	2.88	4.00	2	Two-phase	–
12	Joyo driver	J12	54.5	2.9	0.5	6.43	2.79	3.64	5	Two-phase	–
13	Joyo driver	J13	113.4	3.8	3.4	7.37	−2.01	9.37	6	Two-phase	–
14	Joyo driver	J14	109.2	5.5	1.7	7.03	−2.37	9.40	1	Two-phase	–
15	Joyo driver	J15	65.8	4.2	0.8	6.68	1.18	5.49	1	Two-phase	–
16	Joyo driver	J16	181.4	3.0	0.4	6.81	0.58	6.23	2	Two-phase	–
17	Joyo driver	J17	85.9	3.4	0.5	6.94	3.30	3.64	7	Two-phase	–
18	Joyo driver	J18	84.9	1.5	1.0	6.98	2.43	4.56	16	Two-phase	–
Average of J1–J18			105.3	4.2	1.1	7.0	1.0	6.0			
19	B5D-2	H1	74.2	2.2	0.8	4.80	0.54	4.26	10	Two-phase	–
20	INTA-2	H2	77.4	2.2	0.6	4.63	−0.15	4.78	10	Two-phase	–
21	INTA-2	H3	57.4	0.5	1.0	5.54	0.71	4.83	12	Two-phase	–
Average of H1–H3			69.7	1.6	0.8	5.0	0.4	4.6			

22	B5D-1	M1	58.7	0.6	0.0	8.97	3.58	5.39	10	Three-phase	0.819
23	B5D-2	M2	76.0	3.2	0.0	8.64	4.97	3.67	11	Three-phase	0.841
24	B5D-2	M3	94.9	1.4	0.0	8.44	5.28	3.16	11	Three-phase	0.849
25	INTA-2	M4	84.4	3.9	0.0	8.05	3.28	4.77	13	Three-phase	0.838
26	INTA-2	M5	48.0	0.3	0.0	7.65	2.88	4.77	11	Three-phase	0.843
27	INTA-2	M6	84.5	2.2	0.0	8.42	5.13	3.28	13	Three-phase	0.848
28	INTA-2	M7	58.4	0.8	0.3	7.93	5.57	2.36	12	Three-phase	0.863
Average of M1–M7			72.1	1.8	0.0	8.3	4.4	3.9			0.843
29	B4M	L1	53.9	3.2	0.1	14.17	10.54	3.63	–	Three-phase	0.767
30	B4M	L2	62.8	5.5	0.5	15.60	10.60	5.00	–	Three-phase	0.737
31	INTA-1	L3	64.1	2.4	0.6	14.82	11.22	3.60	3.4	Three-phase	0.759
32	INTA-1	L4	65.6	5.5	0.0	15.81	12.01	3.80	6.8	Three-phase	0.744
Average of L1–L4			61.6	4.2	0.3	15.1	11.1	4.0			0.752
33	INTA-1	L5	106.9	8.0	1.5	14.52	2.66	11.86	3.4	Three-phase	0.676
34	INTA-1	L6	151.7	6.2	0.0	13.96	6.17	7.80	4.0	Three-phase	0.732
Average of L5–L6			129.3	7.1	0.7	14.2	4.4	9.8			0.704
35	P-E01	L7	112.8	11.1	1.4	13.32	0.17	13.15	–	Two-phase	–

[a] In 10000 μm^2.
[b] Area equivalent diameter in ceramographs.

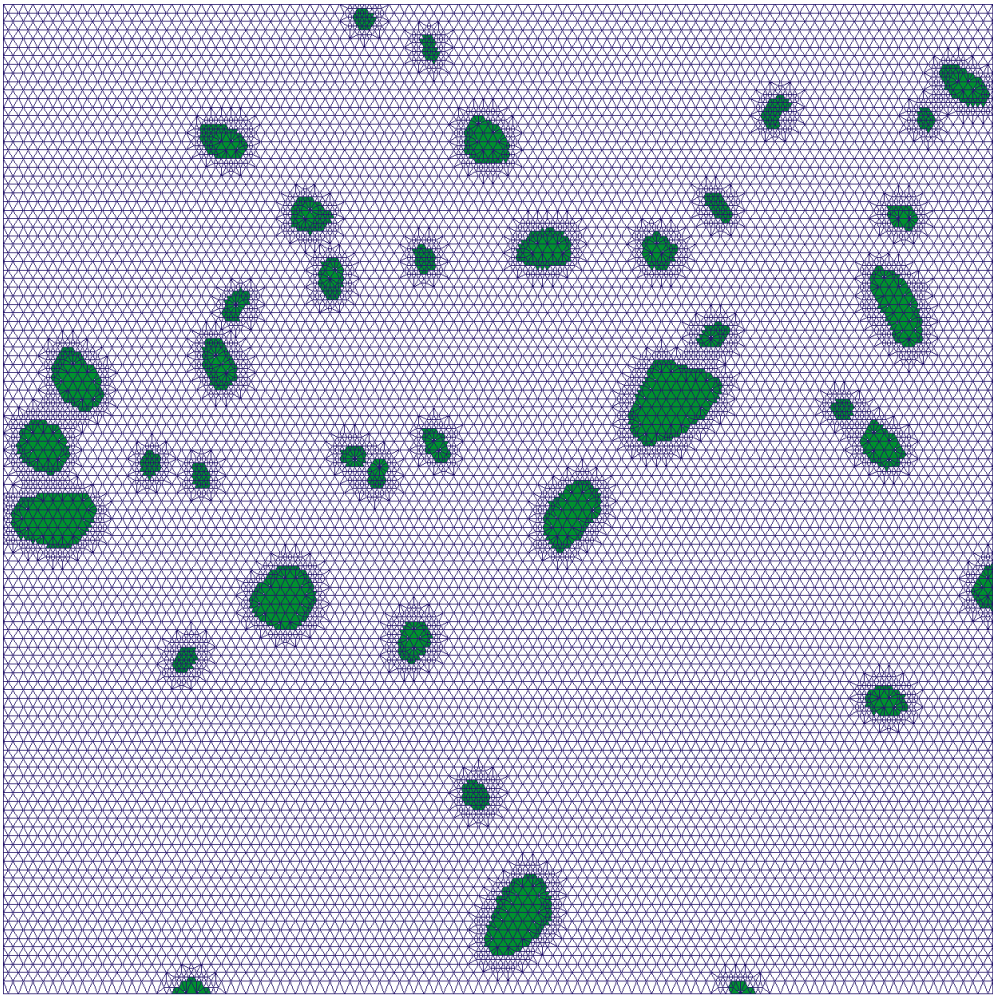

Fig. 5. Matrix and large pore mixtures meshed for FEM analysis (area fraction = 5.0%).

overlaid to determine the porosity effects like, as shown in Fig. 5. The area fraction of porosity ranged from 5.0% to 13.8%. The meshes surrounding pores were re-meshed to minimize the local heat flux induced distortions.

The Inoue's equation [2] for stoichiometric mixed oxide fuel in Eq. (7) was used to calculate the thermal conductivity of the matrix, assuming no radiant heat transfer through the pores:

$$k_0 = \frac{1}{0.01475 + 2.483 \times 10^{-4} T} + 75.27 \times 10^{-12} T^3, \qquad (7)$$

where k_0 is thermal conductivity of fully dense condition in W/mK and T is temperature in K.

In this FEM analysis the heat flows downward and rightward in the squares. In case of the downwards (rightwards) the left and right faces (upper and lower faces) are adiabatic and the upper (left) face is set at 1773 K and the lower (right) face is set at 1273 K.

Figs. 6(a)–(e) show the temperature distribution by the analyses. Analyzed heat flux of each mesh were area-averaged in the square and then divided by ideal heat flux (without porosity), which was the integration of the thermal conductivity: Eq. (7), between 1273–1773 K. The ratio of each area averaged analyzed heat flux to ideal heat flux (F_{2D}) was corrected from the two-dimensional to three-dimensional analytical results (F_{3D}) using the correlation (Eq. (8)) reported by Bakker et al. [17]:

$$\frac{1 - P - F_{2D}}{1 - P - F_{3D}} = 1.8 \pm 0.3, \qquad (8)$$

where P is volume fraction of porosity, F_{2D} is 'analyzed'-to-'ideal' ratio of heat flux in two dimensions, F_{3D}

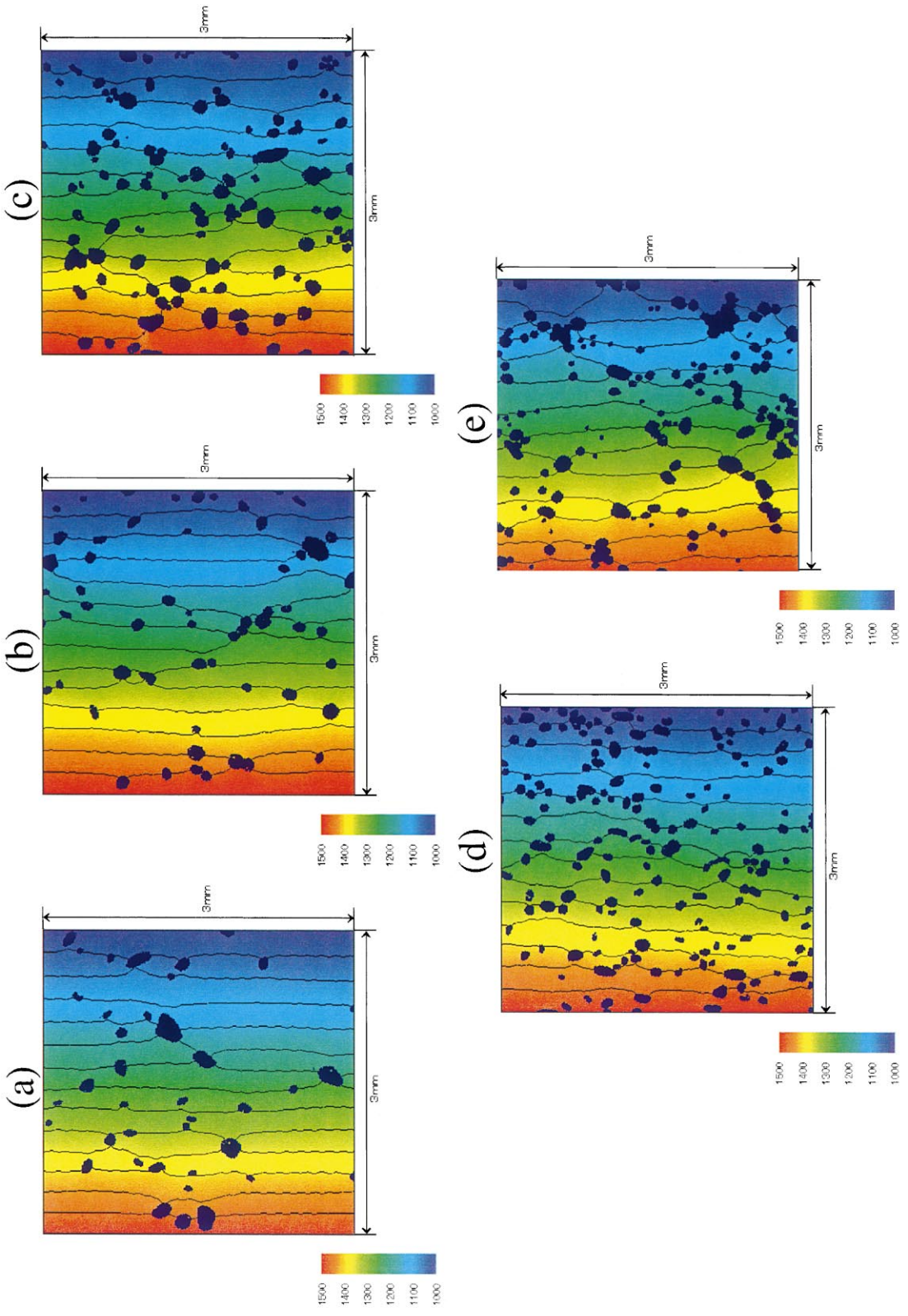

Fig. 6. Temperature distribution in FEM analysis (area fraction (a) = 5.0%; (b) = 6.3%; (c) = 12.5%; (d) = 12.8%; (e) = 13.8%).

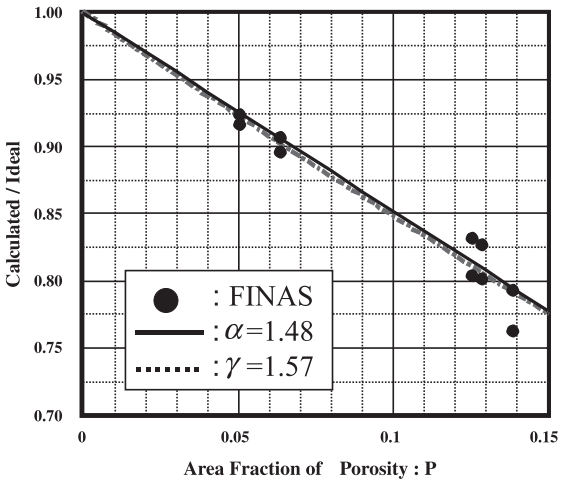

Fig. 7. The effect of large pores on thermal conductivity characterized by FEM analysis.

is 'analyzed'-to-'ideal' ratio of heat flux in three dimensions. F_{3D} were then plotted against the area fraction of the porosity in Fig. 7.

The least square fitting of F_{3D} values of 10 cases of the analyses leads to $\alpha_L = 1.48$, which indicates that large pores thermally behave like as spherical and distributed randomly and that the effect of shape affects little on their matrix in the oxide fuel pellets.

It should be noted that $\alpha_L = 1.48$, which is equivalent to $\gamma = 1.57$, is close to $\gamma = 1.7 \pm 0.2$ reported by Bakker et al. [17] in uranium dioxide after over power transient and also $\gamma = 1.6$ reported by Ikatsu et al. [18] in rim structure.

4. Verification by the measurements

4.1. Thermal conductivity measurements

The thermal conductivity of three lots of the fuel pellets (H1, M3 and L6) was measured to determine the most realistic porosity correction factors and verify the applicability of the method with Eq. (6) developed as described in Section 3.3.

Two specimens were sectioned from fuel pellets of each lot, annealed at 1473 K to recover self-irradiation damage and oxidized to assure stoichiometry (oxygen-to-metal ratio = 2.00). This treatment provided the equivalent basis to characterize only the effect of porosity. The oxygen-to-metal ratio in the specimens was determined by X-ray diffraction techniques before and after the each measurement. Detailed descriptions of the procedures had been already reported by Yamamoto et al. [19,20].

The fuel specimen's thermal diffusivity was measured from 873 to 1873 K, and analyzed by logarithmic methods and converted to thermal conductivity using Eq. (9):

$$k = AC_pD, \tag{9}$$

where k is (effective) thermal conductivity in W/m K, A is thermal diffusivity in m^2/s, C_p is heat capacity [21] in J/kg K, D is density of specimen in kg/m^3.

In Fig. 8 are plotted the results of thermal conductivity measurements and the calculated values from the Philipponneau's Eq. (10) [4], Inoue's Eq. (7) [2], and Inoue's Eq. (11) [3]:

$$k_0 = \frac{1}{0.03616 + 2.493 \times 10^{-4} T} + 88.40 \times 10^{-12} T^3, \tag{10}$$

$$k_0 = \frac{1}{0.06059 + 2.011 \times 10^{-4} T} + \frac{4.715 \times 10^9}{T^2} \exp\left(-\frac{16361}{T}\right), \tag{11}$$

where k_0 is thermal conductivity of fully dense condition in W/m K and T is temperature in K.

4.2. Porosity correction factors by measurements and predictions

A porosity correction factor that is both realistic and reliable can be experimentally determined from the ratio of the measured thermal conductivity to the calculated values from Philipponneau's equation and the Inoue's equations for fully dense fuel, Eqs. (7), (10) and (11), respectively.

Only the ratios above 1200 K, due to their minimal scatter, were averaged as 'experimental factors' and then plotted on ordinate in Fig. 9 to compare with the predicted factors by Eq. (6).

Experimental factors of high-density H1 lot by all three thermal conductivity equations agreed very well with the predicted factor: 0.880 ($P_L = 0$, $P_S = 0.048$, $\alpha_S = 2.5$ in Eq. (6)) as shown in Fig. 9. This confirms that the IAEA recommendation should be used as the coefficient α_S for small pores.

The predicted factors of medium- and low-density fuel lots had been determined with Eq. (6) and listed in Table 2. The average of the predicted factors of fuel lots M1–M7 for M3 (0.843) and the average of the predicted factors of fuel lots L5 and L6 for L6 (0.704) were plotted on abscissa in Fig. 9, since the average of sibling lots may be more realistic. The experimental factors of M3 and L6 also agree very well with the predicted factors as shown in Fig. 9.

As compared above, effective porosity correction factors determined by the method described herein were experimentally verified.

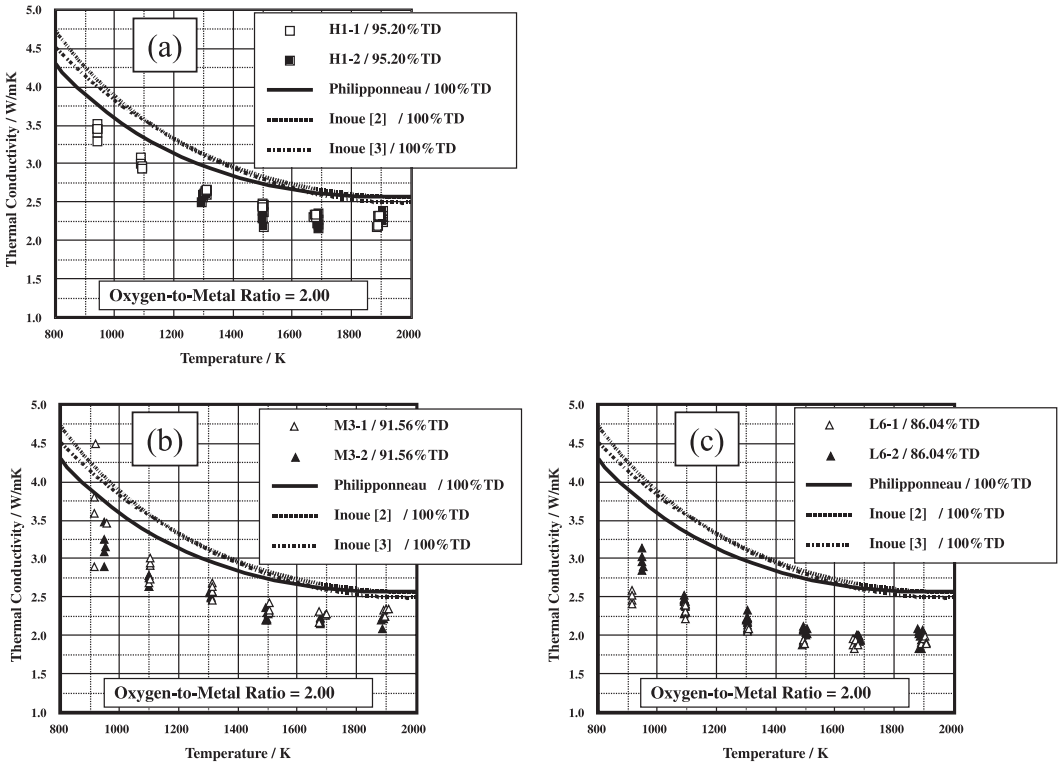

Fig. 8. Experimental results of thermal conductivity measurements for H1, M3 and L6.

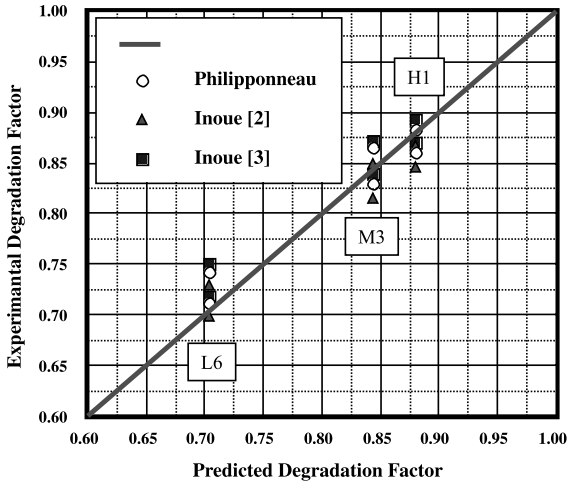

Fig. 9. The effective porosity correction factors determined by measurements and by the prediction method.

5. Conclusion

A reliable method has been developed and verified for determining an effective porosity correction factor for the thermal conductivity of uranium–plutonium oxide fuel pellets.

Fuel pellet morphology can be readily categorized into two types based on pore sizes determined by an image-analysis of ceramographs of random fuel pellet sections. One is a 'two-phase' type that consists of small pores dispersed in the fuel matrix. The other is a 'three-phase' type that has large pores in addition to the small pores dispersed in the fuel matrix. The pore sizes are divided into two categories, large and small, at the 30 μm area equivalent diameter. This method of categorizing the morphology leads to the following equation, which accounts for small and large pore fractions, for determining the effective porosity correction factor by the equation:

$$F = (1 - \alpha_L P_L)(1 - \alpha_S P_S),$$

where F is the effective porosity correction factor; α_S is the coefficient of small pores, α_L is the coefficient of large pores, P_S is the volume fraction of small pores (smaller than 30 μm of area equivalent diameter), and P_L is the volume fraction of large pores (larger than 30 μm of area equivalent diameter).

This study agreed with previous studies on the effect of small pores on thermal conductivity and confirmed that the IAEA recommendation ($\alpha = 2.5$) should be used as the small pore's coefficient α_S. A large pore's coefficient $\alpha_L = 1.48$ was determined by two-dimensional steady-state thermal analysis using FEM code (FINAS).

The validity of this method was demonstrated by comparing it with the measured thermal conductivity of morphology characterized high-, medium-, and low-density fuel pellets.

Acknowledgements

The advices of Naoto Kasahara in FEM analysis and those of Tadashi Maruyama in fuel pellet characterization are gratefully acknowledged. Also the assistance by Junichi Nemoto in image analysis and Sadanori Yasu in FEM analysis are also acknowledged.

References

[1] D.G. Martin, J. Nucl. Mater. 110 (1982) 73.
[2] M. Inoue, T. Mizuno, T. Asaga, PNC TN9410 98-014, 1997.
[3] M. Inoue, T. Asaga, JNC TN9400 98-005, 1998.
[4] Y. Philipponneau, J. Nucl. Mater. 188 (1992) 194.
[5] A.L. Loeb, J. Am. Ceram. Soc. 37 (1954) 96.
[6] B. Schultz, High Temp.–High Press. 13 (1981) 649.
[7] P. Nikolopoulos, G. Ondracek, J. Nucl. Mater. 114 (1983) 231.
[8] Report of the Panel on Thermal Conductivity of Uranium Dioxide held in Vienna in 1965, Technical Reports Series No.59, IAEA, Vienna, 1966.
[9] S. Shimizu, M. Hirai, 1993 Annual Meeting of the Atomic Energy Society of Japan on 27–29 March in Kyoto, Japan, K14, 1993.
[10] Y. Kobayashi, 1988 Fall Meeting of the Atomic Energy Society of Japan on 8–10 October in Hyogo, Japan, H16, 1988.
[11] J.H. Harding, D.G. Martin, P.E. Potter, EUR12402EN, 1989.
[12] I. Unno, T. Kumakura, N. Kushida, S. Ukai, H. Yoshimochi, S. Shikakura, 1992 Annual Meeting of the Atomic Energy Society of Japan on 28–30 March in Kanagawa, Japan, J14, 1992.
[13] M. Soroi, K. Noguchi, H. Kataoka, 1994 Fall Meeting of the Atomic Energy Society of Japan on 28–30 September in Hokkaido, Japan, P2, 1994.
[14] E. Kagota, R. Kitamura, Y. Maeda, 1994 Fall Meeting of the Atomic Energy Society of Japan on 28–30 September in Hokkaido, Japan, P4, 1994.
[15] PNC Techn. Rev. 104 (1997) 67.
[16] K. Iwata, PNC Techn. Rev. 76 (1990) 7.
[17] K. Bakker, H. Kwast, E.H.P. Cordfunke, J. Nucl. Mater. 226 (1995) 128.
[18] N. Ikatsu, N. Itagaki, K. Ohira, K. Bakker, 1988 Fall Meeting of the Atomic Energy Society of Japan on 14–17 October in Okinawa, Japan, L64, 1997.
[19] K. Yamamoto, T. Hirosawa, K. Yoshikawa, K. Morozumi, S. Nomura, J. Nucl. Mater. 204 (1993) 85.
[20] K. Yamamoto, K. Abe, K. Yoshikawa, S. Nomura, PNC ZN9410 93-176, 1993.
[21] J.K. Fink, Int. J. Thermophys. 3 (1982) 165.